2018-01

Applied Reachability Analysis for Spacecraft Rendezvous and Docking with a Tumbling Object

Zagaris, Costantinos; Romano, Marcello

Zagaris, Costantinos, and Marcello Romano. "Applied Reachability Analysis for Spacecraft Rendezvous and Docking with a Tumbling Object." In 2018 Space Flight Mechanics Meeting, p. 2220. 2018.
https://hdl.handle.net/10945/57266

Applied Reachability Analysis for Spacecraft Rendezvous and Docking with a Tumbling Object

Costantinos Zagaris* and Marcello Romano†
Naval Postgraduate School, Monterey, CA, 93943

The objective of this research is to investigate the dynamics, and reachability characteristics of a spacecraft (commonly referred to as the deputy) conducting proximity maneuvers about a resident space object (commonly referred to as the chief) in a tumbling state of motion. Specifically, the goal is to identify initial conditions from which a specified maneuver is feasible, within a specified amount of time. This research question can be answered by solving a reachability problem, and computing a backwards reachable set. However, the complexity of the relative roto-translational dynamics of this scenario poses challenges for existing reachability tools. This paper presents the 6-DOF roto-translational relative spacecraft dynamics, from the perspective of the tumbling chief. A method based on minimum time optimal control is proposed for computation and visualization of backwards reachable sets for both relative translation and rotation, in the particular case of a chief in circular orbit spinning about a principal axis coinciding with the orbit normal. The proposed method makes the problem more tractable and provides insight into the reachability characteristics of this scenario.

Nomenclature

C	=	Chief body-fixed cartesian coordinate system
$C_{\mathsf{A/B}}$	=	Direction cosine matrix describing orientation of reference frame A with respect to reference frame B
D	=	Deputy body-fixed cartesian coordinate system
$\hat{e}$	=	Euler axis of rotation
$\vec{F}$	=	control force vector (N)
$\mathbf{F}_d$	=	control force vector resolved in C (N)
I	=	Earth-centered Inertially fixed cartesian coordinate system
J	=	spacecraft inertia matrix
L	=	Chief local-vertical local-horizontal cartesian coordinate system
m	=	mass (kg)
$\vec{M}$	=	control torque vector resolved in D (N-m)
$\mathbf{M}_d$	=	control torque vector (N-m)
n_c	=	mean motion of chief orbit (rad/s)
q	=	a unit quaternion
$\vec{r}$	=	position vector (m)
$\mathcal{R}_{F(B)}$	=	forward or backward reachable set for specified time T
$\mathbf{v}$	=	relative velocity vector resolved in C (m/s)
$v_{x,\,y,\,z}$	=	components of the relative velocity vector (m/s)
x	=	n-dimensional state vector
$\mathcal{X}$	=	a set of states
u	=	m-dimensional control vector
$\mathcal{U}$	=	a set of admissible control inputs
α	=	Angle of rotation (rad)
γ_Σ	=	an admissible trajectory of the system Σ
μ	=	Earth gravitational constant (m^3/s^2)
$\vec{\rho}$	=	relative position vector (m)

*PhD Candidate, Mechanical and Aerospace Engineering Department, 1 University Circle, Monterey, CA, 93943, and AIAA student member.
†Professor, Mechanical and Aerospace Engineering Department, 1 University Circle, Monterey, CA, 93943, and AIAA Associate Fellow.

$\boldsymbol{\rho}$	=	relative position resolved in C (m)
$\rho_{x,\ y,\ z}$	=	components of the relative position vector (m)
Σ	=	a control affine system
$\boldsymbol{\sigma}$	=	Modified Rodrigues Parameter vector
$\sigma_{1,2,3}$	=	Modified Rodrigues Parameters
$\vec{\omega}_{\mathsf{A/B}}$	=	angular velocity of reference frame A with respect to reference frame B (rad/s)
$\boldsymbol{\omega}$	=	relative angular velocity vector resolved in D (rad/s)
$\boldsymbol{\omega}_c$	=	chief angular velocity resolved in C (rad/s)
$\omega_{x,\ y,\ z}$	=	relative angular velocity components (rad/s)
Ω	=	constant chief rotation rate (rad/s)

I. Introduction

Spacecraft rendezvous and proximity maneuvers are necessary for a variety of space missions, and have been a research topic since the 1960s. Traditionally, the translational and rotational aspects of spacecraft relative motion are treated separately. Relative translational equations describe the relative position/velocity of a deputy spacecraft's center of mass, with respect to a chief spacecraft's center of mass. Relative rotational equations describe relative attitude/angular velocity of the deputy body frame, with respect to the chief body frame, generally assuming the two spacecraft are rigid bodies. When the chief spacecraft is in a tumbling motion, coupling between the translational and rotational states necessitates the use of a 6-Degree-of-Freedom (6-DOF) motion model.

In this paper, we formulate the full 6-DOF relative dynamics, considering a chief spacecraft in a tumbling state. The main focus of this research is to analyze the reachability of the spacecraft relative dynamics, in order to identify initial conditions that allow for a successful maneuver under control and time constraints. The contributions of this work include a backwards reachability analysis of the 6-DOF system, based on solutions to a family of minimum time optimal control problems. The proposed method is used to visualize approximate reachable sets, in lieu of solving the computationally intensive reachability problem. Additionally, a technique is proposed for visualization of backwards reachable sets of spacecraft relative attitudes.

Previous research on the topic of rendezvous with a tumbling object is mainly focused on guidance strategies. Ma *et al.* presented the general formulation of an optimal control problem for a spacecraft to rendezvous with a tumbling satellite in close range, and showed results for a planar case study [1]. Boyarko also presented an optimal control framework for guidance with a tumbling object in a 6-DOF scenario, as well as an Inverse-Dynamics approach for autonomous applications [2, 3]. Boyarko's work was later implemented in a real-time setting, and experimentally demonstrated [4, 5]. Robust control methods for autonomous docking to a tumbling object have also been studied, using sliding mode control [6], and adaptive control [7]. Although research shows a variety of algorithms can be successfully applied to the problem of docking with a tumbling spacecraft, a detailed analysis of the problem has not been presented. This paper aims to fill this gap through reachability analysis.

The topic of reachability is motivated by the need to verify control system behavior and safety. The reachability problem is summarized as follows [8, 9]. Consider a general control-affine system, Σ,

$$\Sigma : \dot{x}(t) = f(x(t), t) + g(x(t), t)u(t), \tag{1}$$

with $x(0) \in \mathcal{X}_0 \subset \mathbb{R}^n$, $x(T) \in \mathcal{X}_f \subset \mathbb{R}^n$, $u(t) \in \mathcal{U} \subset \mathbb{R}^m$, and $t \in [0, T]$. The set of initial conditions ($\mathcal{X}_0$) is used when solving forward reachability problems, while the terminal set ($\mathcal{X}_f$) is used when solving backwards reachability (or controllability) problems. Both sets are assumed to be convex. The set $\mathcal{U}$ represents all admissible controls, and is assumed to be compact and convex. The control input, $u(t)$, is assumed to be a measurable function. Finally, the functions f and g are assumed to be Lipschitz, in order for the dynamics to have a unique solution. The following definitions are written (adapted from [9, 10]).

Definition 1 *An admissible trajectory, $\gamma_\Sigma(0, T)$, is a trajectory of the system, Σ, starting from initial condition $x(0)$, ending at $x(T)$, under admissible control actions $u(t) \in \mathcal{U}$.*

Definition 2 *The forward T-reachable set, $\mathcal{R}_F(T)$, from the initial condition x_0 is the set of states, $x(t)$, that can be reached by admissible trajectories $\gamma_\Sigma(0, T)$ in time $T > 0$ or less:*

$$\mathcal{R}_F(T) = \{x(t) |\ \exists\ \gamma_\Sigma(0, t),\ x(0) = x_0,\ 0 < t \leq T\} \tag{2}$$

Definition 3 *The backwards T-reachable set, $\mathcal{R}_B(T)$, from the final condition x_f is the set of states, $x(0)$, from which admissible trajectories $\gamma_\Sigma(0,T)$ reach x_f in time $T > 0$ or less:*

$$\mathcal{R}_B(T) = \{x(0) | \exists\ \gamma_\Sigma(0,t),\ x(t) = x_f,\ 0 < t \leq T\} \tag{3}$$

In some literature the backwards reachable set is referred to as a controllable set [10, 11], highlighting a relationship between the concepts of controllability and reachability. Fundamentally, controllability analysis is used to determine if an admissible control input can drive the state to some desired location (x_f) in finite time. Controllability analysis is traditionally performed, in a local sense, by examining the Lie structure of the vector fields f and g [9]. This analysis however does not account for constraints on the control variables. Fully answering the question posed in this work, requires computation of the reachable set.

It has been shown that the reachability problem can be posed as an optimal control problem and solved through a particular Hamilton-Jacobi equation [12, 13]. There has been significant efforts in literature focusing on exact computation of reachable sets though numerical solutions of Hamilton-Jacobi equations (see for example [13, 14]), however these methods are computationally intensive and dimensionally limited. Geometric methods for computing reachable sets involve approximating a convex set by a geometric shape (*i.e.* ellipsoid, polytope), and propagating the set according to the system dynamics [15–17]. These approaches require set-based computations, which can be computationally expensive depending on the geometry of the approximate sets [8, 16]. These methods are generally less computationally intensive than exact numerical methods, but could be limited in application (*i.e.* linear systems). Visualization of reachable sets also presents a challenge, as standard plotting tools are limited to three physical dimensions. Some of the above methods have been used in literature for reachability analysis of spacecraft rendezvous missions (see for example [18, 19]), but without considering proximity maneuvering about a tumbling chief.

In our previous work [20], backwards reachable sets were presented for a simplified, planar rendezvous scenario, computed via polytopic approximation methods. Applying those methods to a 6-DOF scenario poses a challenge due to the dimensionality of the state-space, as well as nonlinearity of the dynamics; this paper addresses these challenges. The original contributions of this paper are:

1) Derivation of a decoupled 6-DOF relative motion model, from the perspective of a tumbling chief.
2) Methodology for visualization of backwards T-reachable sets by exploiting time-optimal solutions.
3) Methodology for backwards reachability analysis of relative rotational motion.

In Section II the spacecraft 6-DOF relative motion model to be used in this research is formulated. Section III presents the proposed methodology for visualizing backwards reachable sets. Results are presented in Section IV, and the paper closes with concluding remarks in Section V.

II. Spacecraft Relative Roto-translation Model

Traditionally, spacecraft translational and rotational equations of motion are derived independently. Relative translational equations are generally derived by assuming the spacecraft are point masses. The translational equations of motion are generally nonlinear, but popular linear approximations exist, such as the Clohessy-Wiltshire (CW) model [21]. Spacecraft rotational equations of motion are also inherently nonlinear and derived, for different attitude parametrization schemes, by assuming the spacecraft are rigid bodies [22].

A 6-DOF model can be witten by simply concatenating the translational and rotational equations, as many authors have done in the past (see for example [3, 23]). Other 6-DOF representations seen in literature include a kinematically coupled model, considering the relative motion between off-center-of-mass feature points [24], or using different state representations such as dual quaternions [25]. Traditional equations, however, are not derived from the perspective of a tumbling chief, as proposed here. In this paper, a 6-DOF relative motion model is derived using a rotating reference frame fixed to the tumbling chief spacecraft.

A. Chief Perspective Relative Dynamics

Consider a spacecraft in arbitrary Earth orbit, referred to as the chief, and a controlled spacecraft in a nearby orbit, referred to as the deputy. The following cartesian coordinate systems (CCS) are defined:

- I: Earth-Centered-Inertial reference CCS - origin at the center of the Earth, x axis pointing towards the vernal equinox, z axis toward the North Pole, and y axis completing the right-handed triad

- L: Chief local-vertical, local-horizontal (LVLH), or Hill's CCS - origin at chief's center of mass, x axis pointing radially outward, z axis along orbit normal, and y axis completing the right-handed triad
- C: Chief body-fixed frame, with origin at the chief's center of mass
- D: Deputy body-fixed frame, with origin at the deputy's center of mass

Assume that both spacecraft are rigid bodies. Note that an unresolved geometric vector will be denoted by an arrow over the variable ($\vec{a}$), while a resolved vector in a specified CCS will be denoted by a bold symbol with the CCS indicated as a superscript on the right side ($\mathbf{a}^{\mathsf{C}}$). A superscript on the left side of a variable accompanies a time derivative, indicating the reference frame with respect to which the differentiation is performed (${}^{\mathsf{C}}\dot{\vec{a}}$).

Figure 1 illustrates a depiction of the problem, where $\vec{r}_c$ is the chief's position vector, $\vec{r}_d$ is the deputy's position vector, and $\vec{\rho}$ is the relative position vector of the deputy with respect to the chief. At this time, no assumptions are made about the chief's orbit, and the perturbing forces that may be acting on the two spacecraft are neglected.

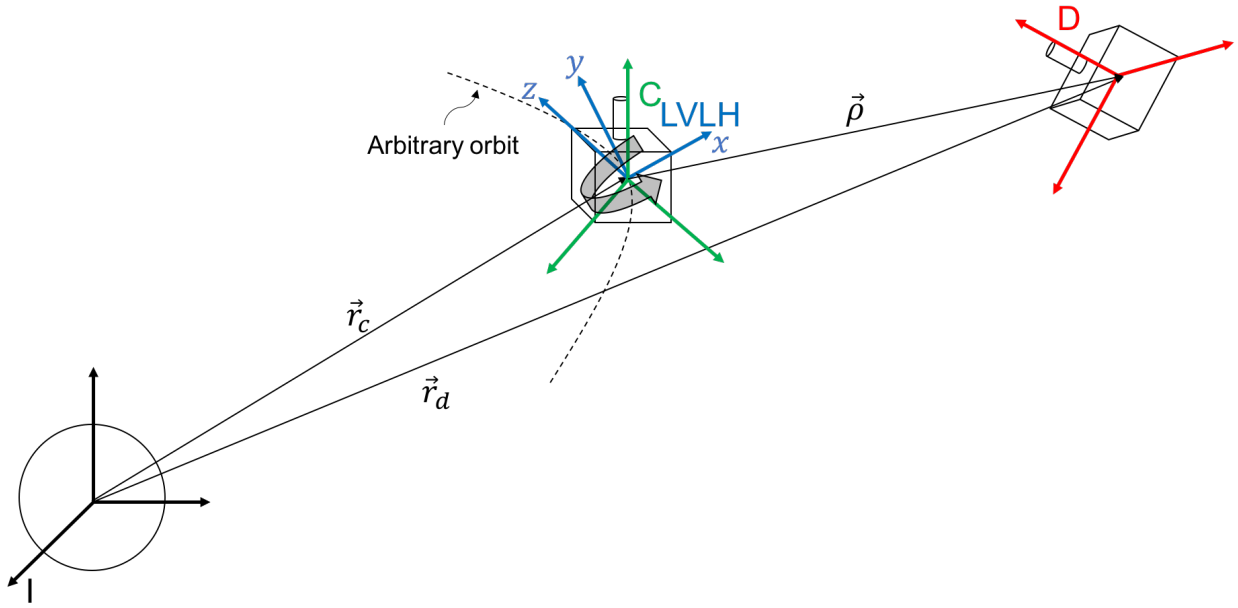

Fig. 1 Vectors and reference coordinate systems for the problem of spacecraft relative motion with respect to a tumbling chief.

1. Relative Translational Motion

First, the relative motion between the centers of mass of the two spacecraft is derived. The chief is assumed to be uncontrolled, with no perturbing forces. The motion of the center of mass of the chief and deputy is described by the two-body orbital equation [21],

$$ {}^{\mathsf{I}}\ddot{\vec{r}}_c = -\frac{\mu}{R_c^3}\vec{r}_c, \tag{4} $$

$$ {}^{\mathsf{I}}\ddot{\vec{r}}_d = -\frac{\mu}{R_d^3}\vec{r}_d + \frac{1}{m_d}\vec{F}_d, \tag{5} $$

where $R_c = ||\vec{r}_c||$, $R_d = ||\vec{r}_d||$, $\vec{F}_d$ is the control force vector acting on the deputy, μ is the Earth's gravitational constant, and m_d is the deputy's mass.

The relative position of the deputy's center of mass with respect to the chief is $\vec{\rho} = \vec{r}_d - \vec{r}_c$. Then,

$$ \begin{aligned} {}^{\mathsf{I}}\ddot{\vec{\rho}} &= {}^{\mathsf{I}}\ddot{\vec{r}}_d - {}^{\mathsf{I}}\ddot{\vec{r}}_c, \\ {}^{\mathsf{I}}\ddot{\vec{\rho}} &= -\frac{\mu}{R_d^3}\vec{\rho} + \frac{\mu\left(R_d^3 - R_c^3\right)}{R_c^3 R_d^3}\vec{r}_c + \frac{1}{m_d}\vec{F}_d. \end{aligned} \tag{6} $$

Using the transport theorem [26], the time derivative of the relative position vector can be taken with respect to C,

$$ {}^{\mathsf{I}}\ddot{\vec{\rho}} = {}^{\mathsf{C}}\ddot{\vec{\rho}} + \dot{\vec{\omega}}_{\mathsf{C/I}} \times \vec{\rho} + 2\vec{\omega}_{\mathsf{C/I}} \times {}^{\mathsf{C}}\dot{\vec{\rho}} + \vec{\omega}_{\mathsf{C}/\mathcal{I}} \times (\vec{\omega}_{\mathsf{C/I}} \times \vec{\rho}), \tag{7} $$

where $\vec{\omega}_{\mathsf{C/I}}$ is the angular velocity of C with respect to I, and $\dot{\vec{\omega}}_{\mathsf{C/I}} = {}^{\mathsf{I}}\dot{\vec{\omega}}_{\mathsf{C/I}} = {}^{\mathsf{C}}\dot{\vec{\omega}}_{\mathsf{C/I}}$. Combining Eq. (6) and Eq. (7) results in the following expression,

$$ {}^{\mathsf{C}}\ddot{\vec{\rho}} = -\frac{\mu}{R_d^3}\vec{\rho} + \frac{\mu\left(R_d^3 - R_c^3\right)}{R_c^3 R_d^3}\vec{r}_c + \frac{1}{m_d}\vec{F}_d - \dot{\vec{\omega}}_{\mathsf{C/I}} \times \vec{\rho} - 2\vec{\omega}_{\mathsf{C/I}} \times {}^{\mathsf{C}}\dot{\vec{\rho}} - \vec{\omega}_{\mathsf{C}/\mathcal{I}} \times (\vec{\omega}_{\mathsf{C/I}} \times \vec{\rho}). \tag{8} $$

Finally, resolving Eq. (8) in C gives the following translational equation of motion,

$$ \ddot{\boldsymbol{\rho}}^{\mathsf{C}} = -\frac{\mu}{R_d^3}\boldsymbol{\rho}^{\mathsf{C}} + \frac{\mu\left(R_d^3 - R_c^3\right)}{R_c^3 R_d^3}\mathbf{r}_c^{\mathsf{C}} + \frac{1}{m_d}\mathbf{F}_d^{\mathsf{C}} - [\dot{\boldsymbol{\omega}}_{\mathsf{C/I}}^{\mathsf{C}}]^{\times}\boldsymbol{\rho}^{\mathsf{C}} - 2[\boldsymbol{\omega}_{\mathsf{C/I}}^{\mathsf{C}}]^{\times}\dot{\boldsymbol{\rho}}^{\mathsf{C}} - [\boldsymbol{\omega}_{\mathsf{C}/\mathcal{I}}^{\mathsf{C}}]^{\times}\left([\boldsymbol{\omega}_{\mathsf{C/I}}^{\mathsf{C}}]^{\times}\boldsymbol{\rho}^{\mathsf{C}}\right), \tag{9} $$

where $[]^{\times}$ is the skew-symmetric matrix representing the vector cross-product operator. It is evident that the translational relative equation in Eq. (9) is coupled to the chief's tumbling motion, given by the rotational equation of motion (Euler's equation) [22],

$$ \dot{\boldsymbol{\omega}}_{\mathsf{C/I}}^{\mathsf{C}} = J_c^{-1}\left(-[\boldsymbol{\omega}_{\mathsf{C/I}}^{\mathsf{C}}]^{\times} J_c \boldsymbol{\omega}_{\mathsf{C/I}}^{\mathsf{C}}\right), \tag{10} $$

where J_c is the chief's inertia matrix. Equation (9) is also a function of the chief's orbital motion (R_c, $\mathbf{r}_c^{\mathsf{C}}$). It is important to note that for an arbitrary chief orbit, the variable R_c is not constant.

2. Relative Rotational Motion

In order to describe the orientation of the deputy with respect to the chief an attitude parametrization scheme must be selected. Unit quaternions are often preferred, from a numerical perspective, as a singularity-free representation of attitude. The unit quaternion, $q_{\mathsf{D/C}}$ describes the orientation of the deputy with respect to the chief and is comprised of a vector part and a scalar part, $q_{\mathsf{D/C}} = [\bar{q}\ q_4]^T = [q_1\ q_2\ q_3\ q_4]^T$, and satisfies $||q_{\mathsf{D/C}}|| = 1$. The quaternion kinematic equation is [22],

$$ \dot{q}_{\mathsf{D/C}} = \frac{1}{2} Q \boldsymbol{\omega}_{\mathsf{D/C}}^{\mathsf{D}}, \tag{11} $$

where

$$ Q = \begin{bmatrix} q_4 & -q_3 & q_2 \\ q_3 & q_4 & -q_1 \\ -q_2 & q_1 & q_4 \\ -q_1 & -q_2 & -q_3 \end{bmatrix}. \tag{12} $$

The relative angular velocity is defined by the following equation,

$$ \vec{\omega}_{\mathsf{D/C}} = \vec{\omega}_{\mathsf{D/I}} - \vec{\omega}_{\mathsf{C/I}}. \tag{13} $$

The relative dynamic equation can then be derived by taking the time derivative of Eq. (13),

$$ {}^{\mathsf{I}}\dot{\vec{\omega}}_{\mathsf{D/C}} = {}^{\mathsf{I}}\dot{\vec{\omega}}_{\mathsf{D/I}} - {}^{\mathsf{I}}\dot{\vec{\omega}}_{\mathsf{C/I}} = {}^{\mathsf{D}}\dot{\vec{\omega}}_{\mathsf{D/I}} - {}^{\mathsf{C}}\dot{\vec{\omega}}_{\mathsf{C/I}}. \tag{14} $$

The attitude dynamic motion of the deputy and chief with respect to the inertial frame (${}^{\mathsf{D}}\dot{\vec{\omega}}_{\mathsf{D/I}}$ and ${}^{\mathsf{C}}\dot{\vec{\omega}}_{\mathsf{C/I}}$ respectively) are defined by Euler's equation [22]. Using the transport theorem, the following equation can be written,

$$ {}^{\mathsf{I}}\dot{\vec{\omega}}_{\mathsf{D/C}} = {}^{\mathsf{D}}\dot{\vec{\omega}}_{\mathsf{D/C}} + \vec{\omega}_{\mathsf{D/I}} \times \vec{\omega}_{\mathsf{D/C}}. \tag{15} $$

Combining Eq. (14) and (15), and plugging in Euler's equation for the deputy rotational motion provides the following equation for the relative rotational motion,

$$ {}^{\mathsf{D}}\dot{\vec{\omega}}_{\mathsf{D/C}} = J_d^{-1}\left[\vec{M}_d - (\vec{\omega}_{\mathsf{D/C}} + \vec{\omega}_{\mathsf{C/I}}) \times J_d(\vec{\omega}_{\mathsf{D/C}} + \vec{\omega}_{\mathsf{C/I}})\right] - {}^{\mathsf{C}}\dot{\vec{\omega}}_{\mathsf{C/I}} - \vec{\omega}_{\mathsf{C/I}} \times \vec{\omega}_{\mathsf{D/C}}, \tag{16} $$

where $\vec{M}_d$ is the control torque applied to the deputy, and J_d is the deputy's inertia matrix. Let $C_{\mathsf{D/C}}$ be the direction cosine matrix corresponding to the unit quaternion $q_{\mathsf{D/C}}$, which transforms a vector from the C CCS to the D CCS. Finally, Eq. (16) can be resolved in D,

$$ \dot{\boldsymbol{\omega}}_{\mathsf{D/C}}^{\mathsf{D}} = J_d^{-1}\left[\mathbf{M}_d^{\mathsf{D}} - [\boldsymbol{\omega}_{\mathsf{D/C}}^{\mathsf{D}} + C_{\mathsf{D/C}}\boldsymbol{\omega}_{\mathsf{C/I}}^{\mathsf{C}}]^{\times} J_d(\boldsymbol{\omega}_{\mathsf{D/C}}^{\mathsf{D}} + C_{\mathsf{D/C}}\boldsymbol{\omega}_{\mathsf{C/I}}^{\mathsf{C}})\right] - C_{\mathsf{D/C}}\dot{\boldsymbol{\omega}}_{\mathsf{C/I}}^{\mathsf{C}} - [C_{\mathsf{D/C}}\boldsymbol{\omega}_{\mathsf{C/I}}^{\mathsf{C}}]^{\times}\boldsymbol{\omega}_{\mathsf{D/C}}^{\mathsf{D}}. \tag{17} $$

As with the translational equation, the attitude equation is a function of the chief's tumbling motion defined in Eq. (10).

3. 6-DOF Relative Roto-Translation Model

For notational compactness the following variables are defined:

- $\boldsymbol{\rho} = \boldsymbol{\rho}^{\mathsf{C}}$; relative position vector resolved in C
- $\mathbf{v} = \dot{\boldsymbol{\rho}}^{\mathsf{C}}$; relative velocity vector resolved in C
- $q = q_{\mathsf{D/C}}$; relative attitude unit quaternion
- $\boldsymbol{\omega}^{\mathsf{D}} = \boldsymbol{\omega}^{\mathsf{D}}_{\mathsf{D/C}}$; relative angular velocity vector resolved in D
- $\mathbf{F}_d = \mathbf{F}^{\mathsf{C}}_d$; control force vector acting on the deputy resolved in C
- $\boldsymbol{\omega}_c = \boldsymbol{\omega}^{\mathsf{C}}_{\mathsf{C/I}}$; chief angular velocity vector resolved in C

The full 6-DOF model describing the relative roto-translational motion of the deputy with respect to the chief is written by Eq. (9), (11), and (17), and shown for completeness in Eq. (18).

$$\dot{\boldsymbol{\rho}} = \mathbf{v} \tag{18a}$$

$$\dot{\mathbf{v}} = -\frac{\mu}{R_d^3}\boldsymbol{\rho} + \frac{\mu\left(R_d^3 - R_c^3\right)}{R_c^3 R_d^3}\mathbf{r}_c^{\mathsf{C}} + \frac{1}{m_d}\mathbf{F}_d - \left[J_c^{-1}\left(-[\boldsymbol{\omega}_c]^{\times} J_c \boldsymbol{\omega}_c\right)\right]^{\times}\boldsymbol{\rho} - 2[\boldsymbol{\omega}_c]^{\times}\mathbf{v} - [\boldsymbol{\omega}_c]^{\times}\left([\boldsymbol{\omega}_c]^{\times}\boldsymbol{\rho}\right) \tag{18b}$$

$$\dot{q} = \frac{1}{2} Q \boldsymbol{\omega}^{\mathsf{D}} \tag{18c}$$

$$\dot{\boldsymbol{\omega}}^{\mathsf{D}} = J_d^{-1}\left[\mathbf{M}_d^{\mathsf{D}} - [\boldsymbol{\omega}^{\mathsf{D}} + C_{\mathsf{D/C}}\boldsymbol{\omega}_c]^{\times} J_d (\boldsymbol{\omega}^{\mathsf{D}} + C_{\mathsf{D/C}}\boldsymbol{\omega}_c)\right] - C_{\mathsf{D/C}}\left[J_c^{-1}\left(-[\boldsymbol{\omega}_c]^{\times} J_c \boldsymbol{\omega}_c\right)\right] - [C_{\mathsf{D/C}}\boldsymbol{\omega}_c]^{\times}\boldsymbol{\omega}^{\mathsf{D}} \tag{18d}$$

The above 6-DOF model is advantageous for reachability computations because the relative translational and rotational states are decoupled. In fact, Eq. (18a) and (18b) do not depend on q and $\boldsymbol{\omega}^{\mathsf{D}}$, and Eq. (18c) and (18d) do not depend on $\boldsymbol{\rho}$ and $\mathbf{v}$. Notably, this is an advantageous consequence of the original choice in this paper of resolving all vectors in the chief's body CCS. Conversely, by following the practive of resolving all vectors in the deputy's CCS the relative motions would become coupled. From a reachability standpoint, it is simpler to study the characteristics of two decoupled subsystems (translational subsystem with 6 states and rotational subsystem with 7 states), rather than a coupled system comprised of 13 states.

B. Simplified Model: Circular chief Rotating in Orbit Plane at Constant Rate

Equation (18) represents the full 6-DOF model for spacecraft relative roto-translation, about a tumbling chief spacecraft in an arbitrary orbit. The only assumptions made in deriving those equations are that the spacecraft are rigid bodies, and no external perturbing forces or torques are acting on the spacecraft (*i.e.* two-body motion). The following additional assumptions are now made to further simplify the problem:

1) Chief spacecraft is in a circular orbit, with mean motion $n_c = \sqrt{\frac{\mu}{R_c^3}}$.
2) Relative distance is small in comparison to the chief's orbit radius, $||\rho|| << R_c$.
3) Chief and Deputy body CCS are aligned with their respective principal axes (*i.e.* J_c and J_d are diagonal).
4) Chief is rotating on the orbit plane, about its z-body axis, at a constant rate, Ω.
5) Chief body CCS is initially aligned with the LVLH CCS (L).

With the above assumptions, the chief's orbital and attitude parameters can be written as follows,

$$\boldsymbol{\omega}_c = \begin{bmatrix} 0 \\ 0 \\ \Omega + n_c \end{bmatrix}, \quad \mathbf{r}_c^{\mathsf{C}} = \begin{bmatrix} R_c \cos\Omega t \\ -R_c \sin\Omega t \\ 0 \end{bmatrix}. \tag{19}$$

Consider the state vector $x = [\boldsymbol{\rho},\ \mathbf{v}]^T = [\rho_x\ \rho_y\ \rho_z\ v_x\ v_y\ v_z]^T \in \mathbb{R}^6$, made up of the relative position and velocity, and control vector $u = \mathbf{F}_d \in \mathbb{R}^3$. Plugging Eq. (19) into Eq. (18b), and linearizing the result about the origin, results in the linear time-varying system, describing the relative translational motion,

$$\dot{x}(t) = A(t)x(t) + Bu(t), \tag{20}$$

with

$$A(t) = \begin{bmatrix} 0 & 0 & 0 & 1 & 0 & 0 \\ 0 & 0 & 0 & 0 & 1 & 0 \\ 0 & 0 & 0 & 0 & 0 & 1 \\ 3n_c^2 \cos\Omega t + \Omega^2 + 2\Omega n_c & 0 & 0 & 0 & 2(\Omega + n_c) & 0 \\ 0 & \Omega^2 + 2\Omega n_c & 0 & -2(\Omega + n_c) & 0 & 0 \\ 0 & 0 & -n_c^2 & 0 & 0 & 0 \end{bmatrix}, \tag{21}$$

and

$$B = \frac{1}{m_d} \begin{bmatrix} 0_{3\times3} \\ I_3 \end{bmatrix}, \tag{22}$$

where I_3 is the 3-by-3 identity matrix. Note that the out-of-plane motion ($\rho_z,\ v_z$) is decoupled from the in-plane motion. Additionally, in the case where the chief is not rotating ($\Omega = 0\ deg/s$), Eq. (20) reduces to the traditional CW equations. Although this equation is an approximation of the nonlinear equation of motion, the approximation remains fairly accurate at small relative distances, as in the case of the traditional CW equations.

The relative rotational subsystem, Eq. (18c) and (18d), could be simplified by linearizing the equations about an equilibrium. However, this approximation is only accurate around the equilibrium point (*i.e.* small angular displacements) which does not provide insight in terms of reachability. Therefore, the nonlinear equations are used to analyze the reachability properties of the relative rotational subsystem.

III. Reachability Analysis Methodology

The goal of this paper is to compute and visualize backwards T-reachable sets (recall Definition 3) for the simplified translational subsystem shown in Eq. (20), and the rotational subsystem in Eq. (18c) and (18d), and observe how the sets change as the chief's rotation rate increases. The control constraints are assumed to be of the form, $||u||_\infty \leq u_{max}$, which in this case restricts each component of the translational control force, and torque, to be below a given value.

The translational subsystem, although linear, is time-varying which prevents the use of polytopic approximation methods used in our previous work [20, 27], and the relative attitude subsystem is nonlinear. Level-set methods [13, 14] would also be challenging to implement due to the dimensionality of these subsystems. Additionally, maneuver times for spacecraft applications can be large posing an additional challenge for numerical computation of reachable sets.

The relationship between time-optimal control solutions and the reachable sets can be exploited to gain insight into the reachability characteristics of this complex scenario. Consider the general control-affine system shown in Eq. (1), and let x_0 denote the initial state and x_f denote the desired final state. The time-optimal solution, if it exists, is the admissible trajectory from x_0 that reaches x_f in minimum time, T^*. This solution can be visualized as the earliest instant at which the forward T-reachable set from x_0 includes the state x_f [28]. In other words, x_f is on the boundary of the forward reachable set corresponding to time T^*: $x_f \in \partial\mathcal{R}_F(T^*)$. A dual correspondence can be made to relate time-optimal solutions to a backwards reachable set. The time-optimal solution can be visualized as the earliest instant at which the backwards T-reachable set from x_f includes x_0. More precisely, x_0 is on the boundary of the backwards reachable set corresponding to time T^*: $x_0 \in \partial\mathcal{R}_B(T^*)$. This relationship between reachable sets and time-optimal control offers the following insight.

Remark 1 *The boundary of the backwards T-reachable set is made up of all initial conditions from which admissible trajectories reach the target state in minimum time, T; this is also known as a minimum isochrone [28].*

$$\partial\mathcal{R}_B(T) = \{x_0 \mid \gamma_\Sigma(0,T),\ x(T) = x_f,\ T = \textit{minimum time to reach } x_f\} \tag{23}$$

As a result, the boundary of a backwards reachable set can be visualized by contours of minimum time solutions over the state space. This method enables visualization of an approximate reachable set in a subspace of interest. A set of initial conditions, x_0, is created over the subspace (*e.g.* varying position variables while keeping initial velocities constant). The minimum time optimal control problem, with appropriate constraints, is evaluated for each test point using GPOPS-II [29]. Contours of the minimum time solutions are plotted over the desired subspace, representing slices of the backwards reachable sets with time corresponding to the specified contour levels. Although this method is still computationally intensive, it makes the problem more tractable, and enables visualization of backwards reachable sets to gain insight into the problem of spacecraft rendezvous with a tumbling object.

IV. Results: Chief Rotating in Orbit Plane at Constant Rate

As described in Section III, minimum time solutions are utilized to create an approximation of the boundary of a backwards reachable set. The scenario used in this paper includes an uncontrolled chief, in circular orbit, rotating on the orbit plane at a constant rate, Ω. Backwards reachability is analyzed for different chief rotation rates, and time intervals. First, the translational subsystem is analyzed, followed by analysis of the rotational subsystem. The scenario parameters are shown in Table 1. The optimal control problems required to visualize the minimum time contours for these subsystems are solved using the High Performance Computing (HPC) cluster at the Naval Postgraduate School.

Table 1 Scenario Parameters

Chief Orbit Altitude (km)	400
Chief Mass (kg)	100
Deputy Mass (kg)	100
Chief Inertia (kg-m^2)	$diag(16.67,\ 16.67,\ 16.67)$
Deputy Inertia (kg-m^2)	$diag(16.67,\ 16.67,\ 16.67)$
F_{max} (N)	1
M_{max} (N-m)	1
T_{max} (s)	1000
Desired final condition	$\boldsymbol{\rho}_f = [1, 0, 0]^T\ m$
	$\mathbf{v}_f = [0, 0, 0]^T\ m/s$
	$q_f = [0, 0, 0, 1]^T$, or $\boldsymbol{\sigma}_f = [0, 0, 0]^T$
	$\boldsymbol{\omega}_f = [0, 0, 0]^T\ rad/s$

A. Analysis of the Translational Backwards Reachability

The translational subsystem is the 6-dimensional system shown in Eq. (20), with state vector $x = [\boldsymbol{\rho},\ \mathbf{v}]^T = [\rho_x\ \rho_y\ \rho_z\ v_x\ v_y\ v_z]^T$, and control vector $u = \mathbf{F}_d$, with constraint $||u||_\infty \leq F_{max}$. Since the out-of-plane motion ($\rho_z,\ v_z$) is decoupled, it can be analyzed independently from the planar motion.

The two-dimensional out-of-plane motion is time-invariant and not dependent on the chief's rotation rate. A set of 1,000 test initial conditions is created in the following subspace: $-100\ m\ \leq \rho_z \leq 100\ m$, and $-1\ m/s\ \leq v_z \leq 1\ m/s$. The minimum time optimal control problem is attempted from each of the conditions. The resulting minimum time contours are shown in Fig. 2. The approximate shape of the backwards reachable sets becomes apparent, and it can be seen that the sets grow proportionally with time.

The four-dimensional planar motion poses a dimensionality problem for visualization. In this case, subspaces are created representing slices of the four-dimensional sets. The first slice is defined by 2,500 test initial conditions in the following subspace: $-100\ m\ \leq (\rho_x,\ \rho_y) \leq 100\ m$, at $\mathbf{v} = [0, 0]^T$. Recall that the relative velocity is resolved in the chief's rotating body frame; as such, zero relative velocity imposes an initial inertial velocity on the deputy due to the chief's orbital and rotating motion. The minimum time optimal control problem is attempted for each test point with chief rotation rates of $\Omega = 0,\ 2,\ 4$, and 6 degrees per second (total of 10,000 runs). Figure 3 shows the resulting minimum time contours. As the chief's rotation rate increases, the solver encounters more infeasibilities, apparent by the missing contours in Fig. 3(d), indicating that the maneuver becomes more difficult at higher rotation rates. The contours also increase proportionally with time and shrink as the target's rotation rate increases.

The second slice of the four-dimensional set to be examined is defined by 2,500 test initial conditions in the following subspace: $-100\ m\ \leq (\rho_x,\ \rho_y) \leq 100\ m$, at an initial relative velocity corresponding to the deputy spacecraft being in a Natural Motion Circumnavigation (NMC) trajectory, transcribing a 2-by-1 ellipse around the chief. For each test point this initial relative velocity is given by,

$$\mathbf{v}_0 = \begin{bmatrix} \frac{1}{2} n_c \rho_y \\ -2 n_c \rho_x \\ 0 \end{bmatrix} - [\boldsymbol{\omega}_c]^\times \begin{bmatrix} \rho_x \\ \rho_y \\ 0 \end{bmatrix}, \tag{24}$$

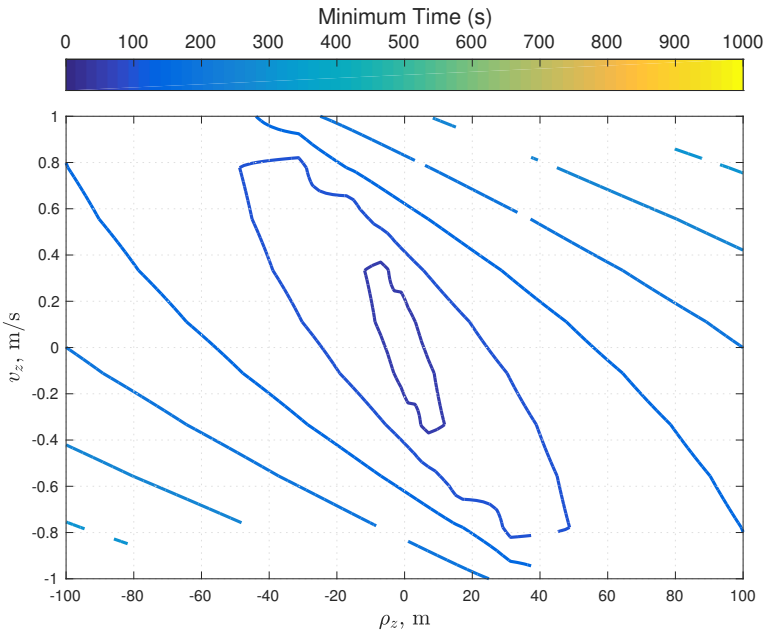

Fig. 2 Out-of-plane slice of backwards T-reachable set; color bar indicates minimum time values corresponding to the contours.

where recall n_c is the chief's orbital mean motion, and $\boldsymbol{\omega}_c$ is the chief's angular velocity given in Eq. (19). Note that in Eq. (24) the chief's rotating motion is accounted for in order to express the NMC initial velocity in C. The resulting minimum time contours are shown in Fig. 4. In this case, as the chief rotation rate increases the sizes of the contours do not change significantly, and the time values represented in Fig. 4(a) - 4(d) remains the same. This is due to the fact that the initial velocity includes the rotation of the chief. As opposed to the zero velocity subspace, depicted in Fig. 3, there is no dramatic loss of maneuver feasibility in the NMC subspace, with chief rotation rate up to 6 deg/s.

Next, backwards reachability characteristics are analyzed in the initial velocity subspace, while keeping relative initial position constant. The third slice of the four-dimensional backwards reachable set is defined by 2,500 test initial conditions in the following subspace: $-10\ m/s\ \leq (v_x,\ v_y) \leq 10\ m/s$, at an initial relative position on the V-bar (y) axis, $\boldsymbol{\rho} = [0,\ 100]^T\ m$. The resulting minimum time contours are shown in Fig. 5. It can be seen that as the chief rotation rates increases the contours move towards the right side of the plot, and are almost off the figure in Fig. 5(d). This behavior shows that at higher chief rotation rates, the deputy needs a larger initial relative velocity along the x direction in order to complete the maneuver successfully.

Finally, the fourth slice of the four-dimensional set to be examined is defined by 2,500 test initial conditions in the following subspace: $-10\ m/s\ \leq (v_x,\ v_y) \leq 10\ m/s$, at an initial relative position on the R-bar (x) axis, $\boldsymbol{\rho} = [100,\ 0]^T\ m$. The resulting minimum time contours are shown in Fig. 6, showing a similar trend as the V-bar sets in Fig. 5. In this case, the contours move towards the bottom of the plot showing that for higher chief rotation rates the deputy requires larger initial velocity in the y direction.

The above analysis of the translational subsystem shows some characteristics and limitations of the rendezvous maneuver. The results show expected behavior of sets growing proportionally with time, since the system is linear. It is evident that some of the test cases were not able to be solved, especially at increased rotation rates. Many of the cases become infeasible, in the sense that the maneuver is not possible within the allowable 1,000 seconds. Some of the infeasibilities, however, could be an artifact of the nonlinear programming solver setup, and user-defined parameters within GPOPS-II.

B. Analysis of the Rotational Backwards Reachability

The rotational subsystem is the seven-dimensional system in Eq. (18c)-(18d), with state vector $x = [q,\ \boldsymbol{\omega}]^T$ and control vector $u = \mathbf{M}_d$, with constraint $||u||_\infty \leq M_{max}$. The rotational dynamics is nonlinear, and defining slices of

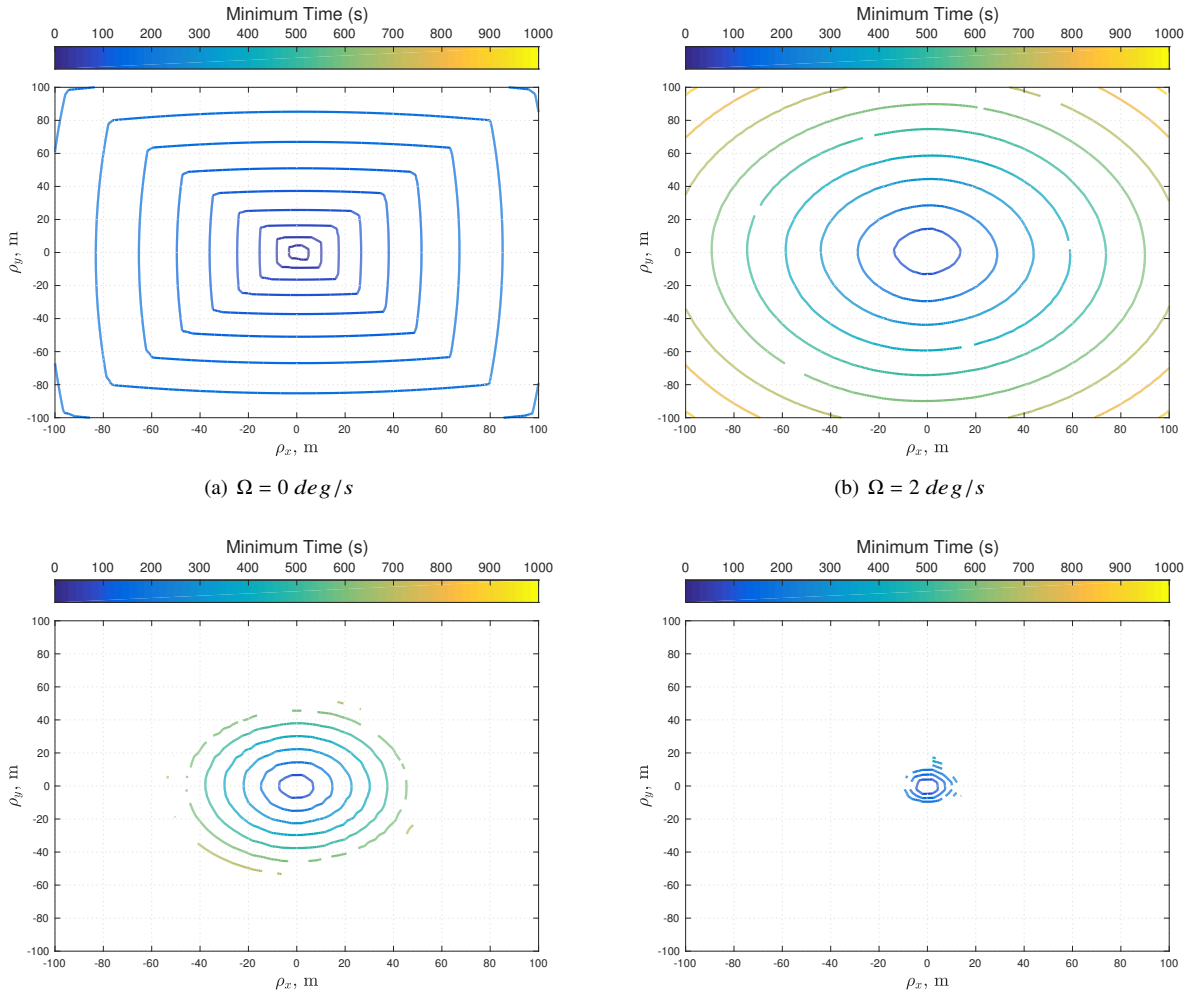

(a) $\Omega = 0\ deg/s$

(b) $\Omega = 2\ deg/s$

(c) $\Omega = 4\ deg/s$

(d) $\Omega = 6\ deg/s$

Fig. 3 Translational backwards T-reachable set slices at zero initial relative velocity, at different chief rotation rates; color bar indicates minimum time values corresponding to the contours.

a set of relative attitudes is a complicated problem. Since quaternions are used as the parametrization of rigid body attitudes, a set of quaternions is four-dimensional and impossible to plot. Additionally, even if it could be plotted, the insight gained from this plot would be limited as quaternions are not intuitive. A visualization technique for backwards reachable relative attitude sets is proposed herein.

First, a four-dimensional subspace of the seven-dimensional state space is created by selecting a random uniform distribution of 1,000 initial unit quaternions, using the procedure outlined in [30], while keeping a constant initial relative angular velocity, $\boldsymbol{\omega} = [0, 0, 0]^T$. The minimum time optimal control problem is attempted for each test point, at chief rotation rates $\Omega = 0,\ 2,\ 4$, and 6 degrees per second (total of 4,000 runs). The Modified Rodrigues Parameters (MRP) are used as an alternative to quaternions for visualization of the backwards reachable sets. The MRP vector, $\boldsymbol{\sigma} = [\sigma_1,\ \sigma_2,\ \sigma_3]^T$, is a stereographic projection of the set of unit quaternions (four-dimensional unit sphere) onto a particular hyperplane [26]. The MRPs are given by,

$$\sigma_i = \frac{q_i}{1 + q_4},\ i = 1,\ 2,\ 3. \tag{25}$$

MRPs can also be expressed in terms of a principal rotation by,

$$\boldsymbol{\sigma} = \hat{e} \tan \frac{\alpha}{4}, \tag{26}$$

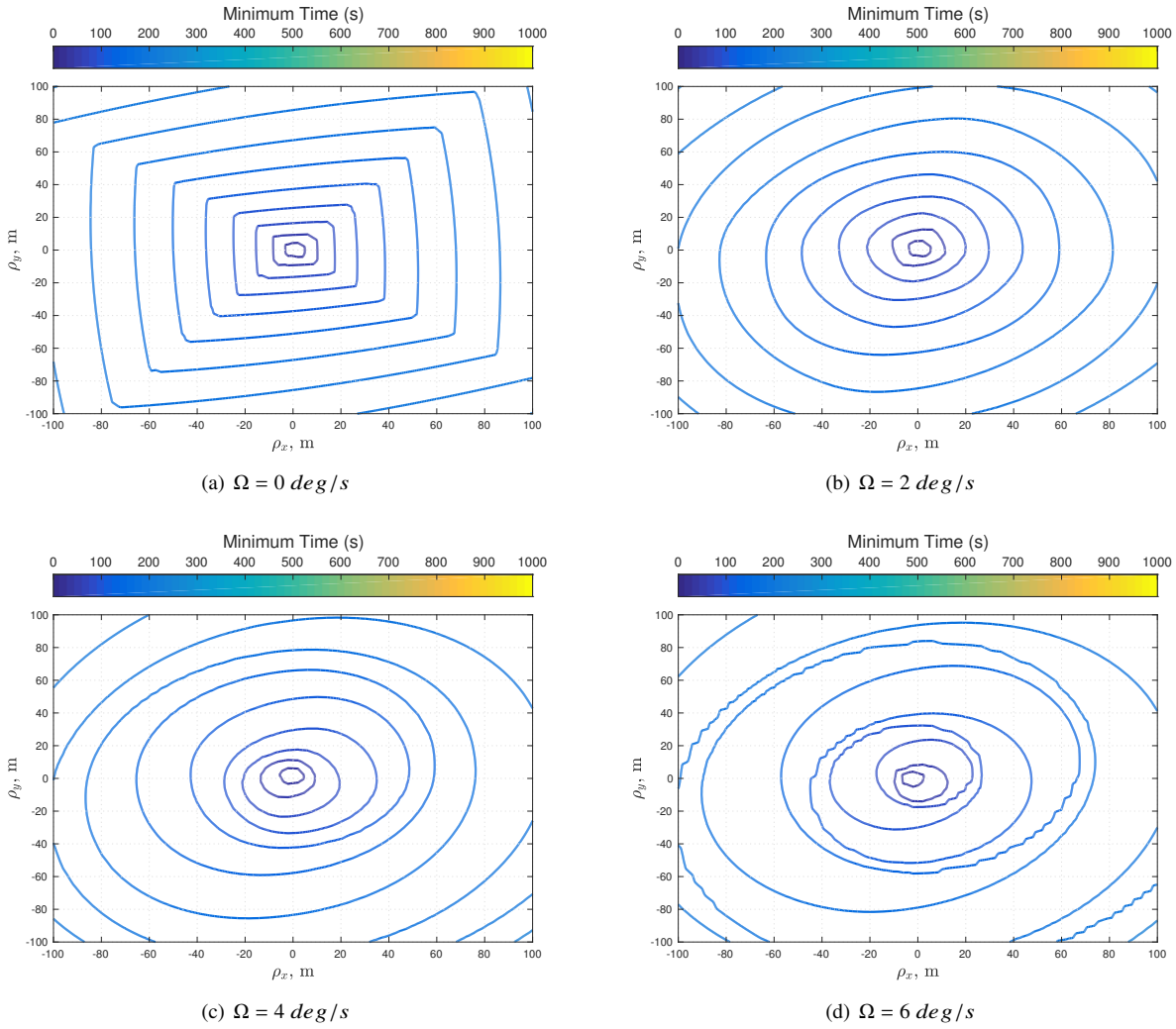

(a) $\Omega = 0\ deg/s$

(b) $\Omega = 2\ deg/s$

(c) $\Omega = 4\ deg/s$

(d) $\Omega = 6\ deg/s$

Fig. 4 Translational backwards T-reachable set slices at NMC initial relative velocity, at different chief rotation rates; color bar indicates minimum time values corresponding to the contours.

where $\hat{e}$ is the Euler axis of rotation, and α is the rotation angle. MRPs have a singularity at $\alpha = \pm 2\pi$. Additionally, the shadow MRP, $\boldsymbol{\sigma}^S$, corresponding to the orientation given by $-q$ (which is equivalent to the orientation given by q), is a distinct set of parameters representing the same orientation. This characteristic allows to switch between $\boldsymbol{\sigma}$ and $\boldsymbol{\sigma}^S$ at $\alpha = \pi$ (*i.e* orientations with $\alpha \leq \pi$ are represented by $\boldsymbol{\sigma}$, while orientations with $\alpha > \pi$ are represented by $\boldsymbol{\sigma}^S$). As a result, the norm of the MRP vector is bounded, $0 \leq \boldsymbol{\sigma}^T\boldsymbol{\sigma} \leq 1$ [26].

By Eq. (26) it is evident that the MRP vector is related to the location of the Euler axis, while the norm ($\boldsymbol{\sigma}^T\boldsymbol{\sigma}$) is related to the rotation angle. Each of the 1,000 test points has a corresponding $\boldsymbol{\sigma}$ (or $\boldsymbol{\sigma}^S$ depending on the rotation angle) and minimum time solution associated with it, resulting in a three-dimensional volume. The MRP norm represents a sphere of a particular radius, which is used as a slicing surface. Backwards reachable sets of relative attitudes can be visualized by projecting minimum time contours in the MRP subspace onto a sphere of a particular radius (between 0 and 1). A point on this sphere represents the location of the Euler axis, while the size of the sphere represents the rotation angle. This technique provides an intuitive visualization of a set of attitudes.

Figure 7 shows the minimum time contours for different values of the MRP norm, in the case of $\Omega = 0\ deg/s$. It can be seen that as the sphere radius grows, representing larger rotations, the minimum time values indicated by the contours grows which is an expected result; larger rotational maneuvers will take a longer time to complete. In Fig. 7(c) some peaks become visible on the southern hemisphere, representing initial relative attitudes on the edge of the backwards

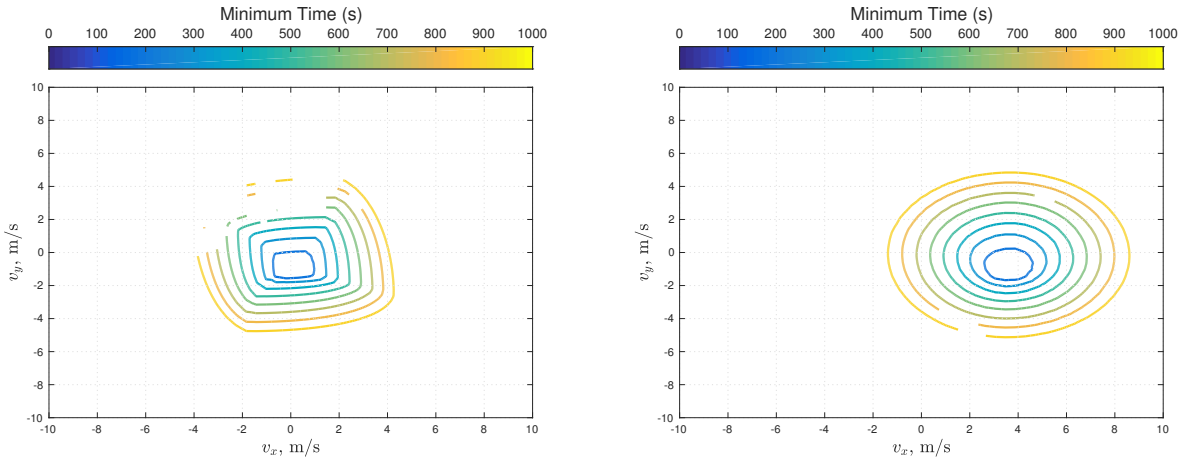

(a) $\Omega = 0\ deg/s$ (b) $\Omega = 2\ deg/s$

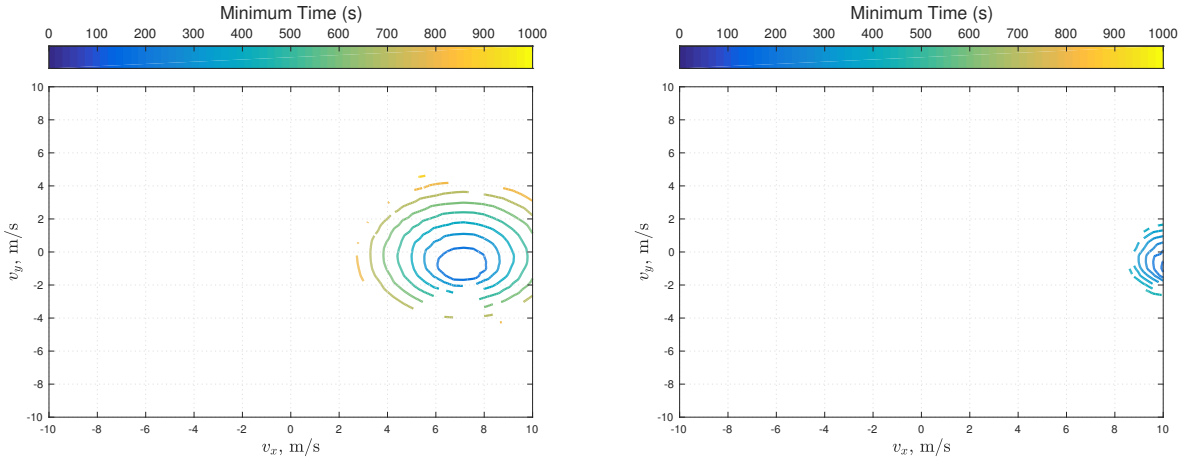

(c) $\Omega = 4\ deg/s$ (d) $\Omega = 6\ deg/s$

Fig. 5 Translational backwards T-reachable set slices at an initial relative position on the V-bar axis, at different chief rotation rates; color bar indicates minimum time values corresponding to the contours.

reachable set for this case. It is evident that the projections are not fully populated, indicating that 1,000 test points is not enough. More test cases would be necessary to get the full picture, but even this limited data set is enough to offer some insight.

Figures 8 - 10 show the resulting minimum time contours as the chief rotation rate increases from $\Omega = 2\ deg/s$ to $\Omega = 6\ deg/s$. These figures show a similar trend of larger time values as the sphere radius grows. Additionally, comparing to the time values seen in the zero chief rotation case, Fig. 7(c), as the chief rotation rate increases contours of larger time values become visible. The overwhelming result seen in these figures is that 1,000 test points is not enough to get a full picture. It may be more beneficial to use a more strategic selection of test points, instead of using a randomized placement method.

Finally, the backwards reachability of the relative attitude dynamics is examined in the three-dimensional angular velocity subspace. This subspace is defined by 1,000 test points with $-30\ deg/s \leq (\omega_x,\ \omega_y,\ \omega_z) \leq 30\ deg/s$, at an initial relative quaternion $q = [0,\ 0,\ 0,\ 1]^T$; the deputy is initially aligned with the chief. The minimum time optimal control problem is again attempted for each of these test points, at chief rotation rates $\Omega = 0,\ 2,\ 4,$ and 6 degrees per second (total of 4,000 runs). To visualize these results slices are created along the ω_x and ω_y variables, at a specified value of ω_z. The resulting contours at $\omega_z = 0\ deg/s$ are shown in Fig. 11. Figures 12 and 13 show results for $\omega_z = -15$ and $15\ deg/s$, respectively.

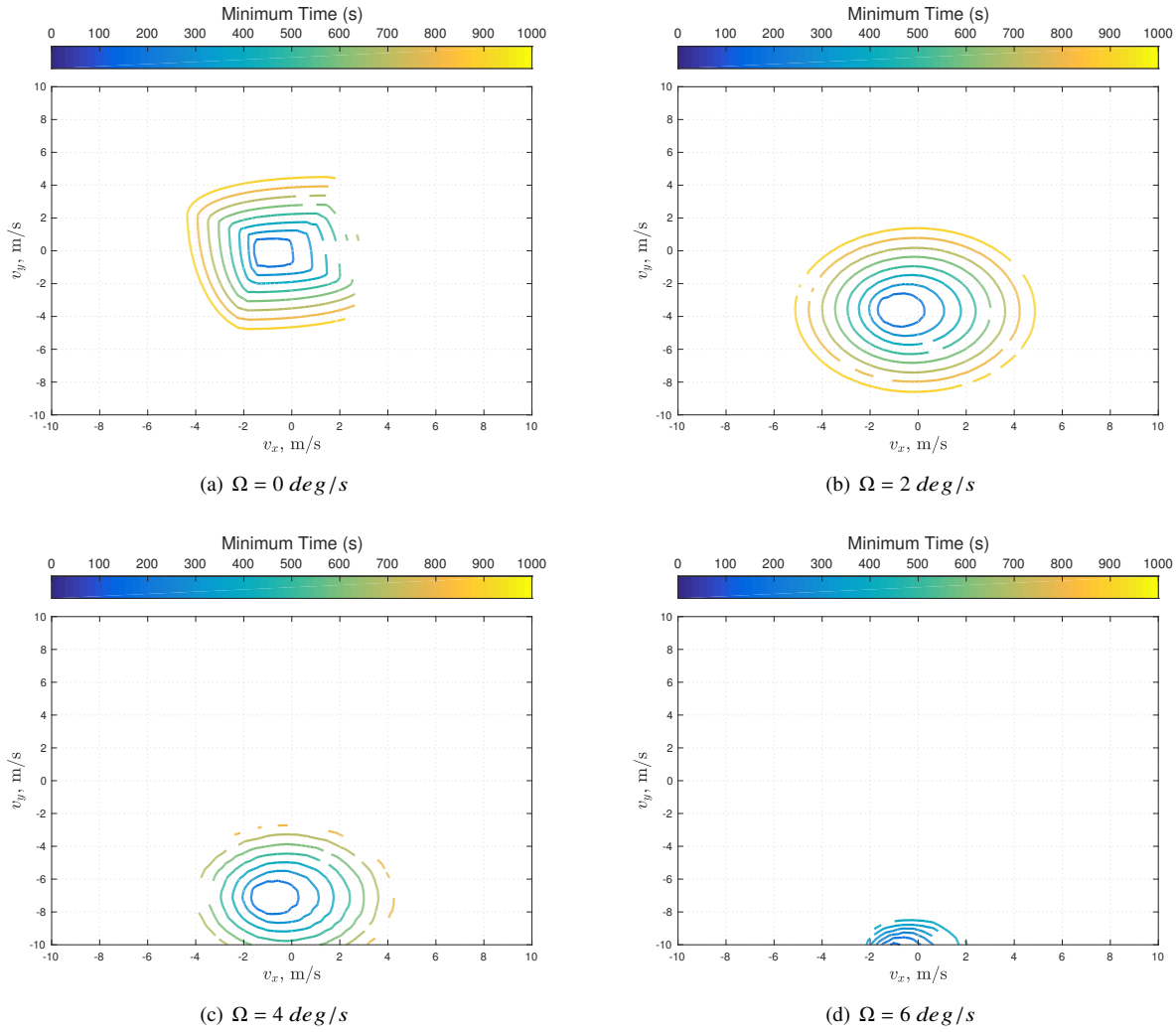

(a) $\Omega = 0\ deg/s$

(b) $\Omega = 2\ deg/s$

(c) $\Omega = 4\ deg/s$

(d) $\Omega = 6\ deg/s$

Fig. 6 Translational backwards T-reachable set slices at an initial relative position on the R-bar axis, at different chief rotation rates; color bar indicates minimum time values corresponding to the contours.

An interesting characteristic that becomes evident in Fig. 11 - 13 is that around the origin, the contours grow proportionally with time. This indicates that the behavior of the attitude dynamics around the origin is similar to that of a linear system. In regions further away from the origin, where a linear approximation would not be accurate, the contours show more complex behavior with multiple peaks. This linear region seems to be approximately contained within $\pm 0.2\ rad/s$. Comparing Fig. 11 - 13 reveals that the contours do not change very much at different levels of ω_z. Also, comparing the four subfigures within Fig. 11 - 13 shows that as the chief rotation rate increases the contours do not change significantly. This behavior is likely due to the high maximum allowable torque, in relation to the deputy's relatively small inertia. It is worth noting, however, that the solver encountered more infeasible cases at the higher rotation rates, as can be seen for example by the missing contours in Fig. 13(c) and 13(d).

The backwards reachability analysis of the relative attitude subsystem is more complex than the translational system analysis. Reachability analysis of spacecraft reorientation maneuveres, in general, has not been seen in literature. This is likely due to the complexity of the dynamics, as evidenced here. As a result, there is not an intuitive expectation of what the results should present. The technique for visualization presented above, however, provides insight into the capabilities of the system. It becomes overwhelmingly obvious that more data is needed to draw better conclusions about this complex scenario.

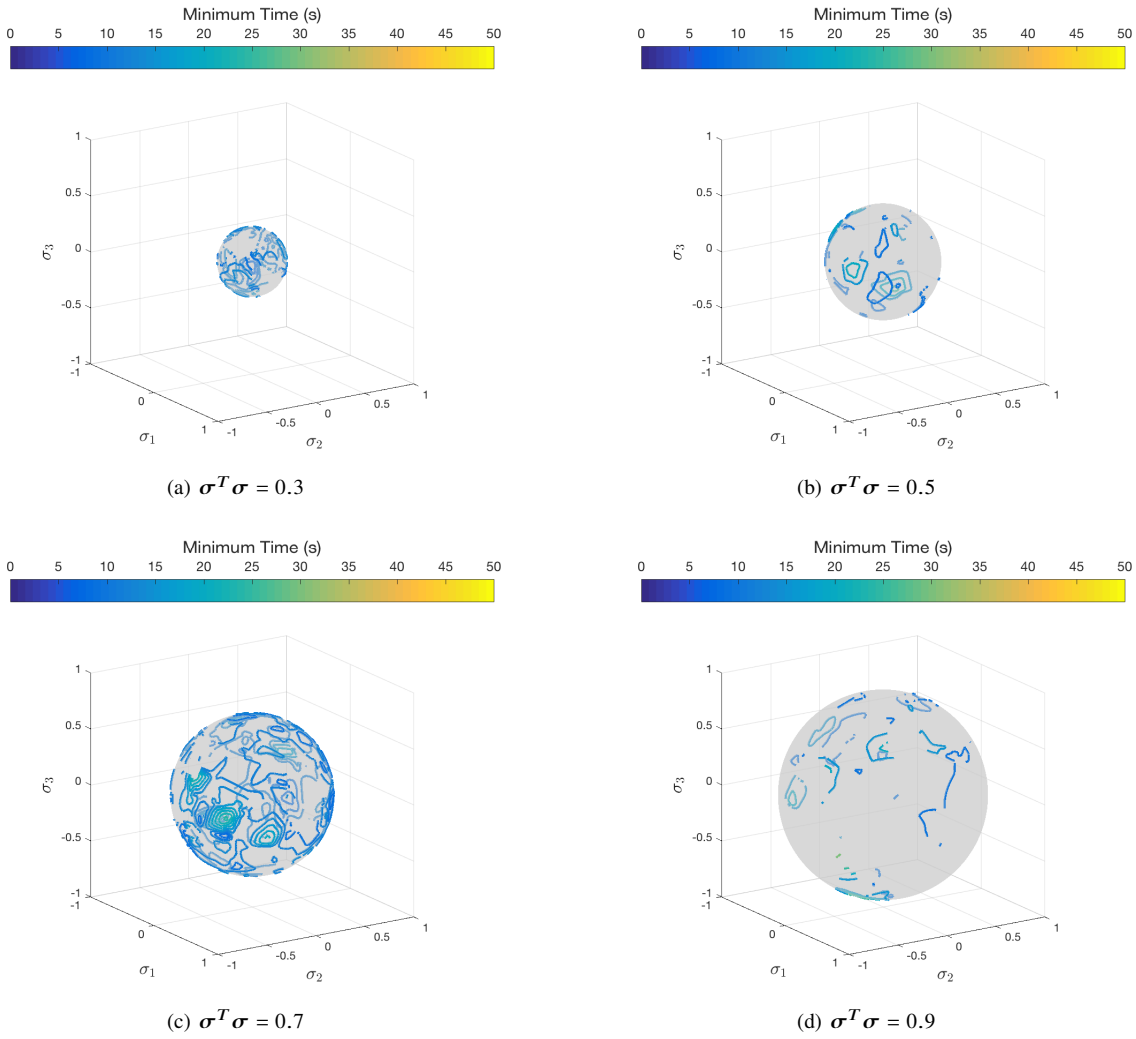

(a) $\boldsymbol{\sigma}^T\boldsymbol{\sigma} = 0.3$ (b) $\boldsymbol{\sigma}^T\boldsymbol{\sigma} = 0.5$

(c) $\boldsymbol{\sigma}^T\boldsymbol{\sigma} = 0.7$ (d) $\boldsymbol{\sigma}^T\boldsymbol{\sigma} = 0.9$

Fig. 7 Rotational backwards T-reachable set slices at zero initial relative angular velocity, at $\Omega = 0\ deg/s$; color bar indicates minimum time values corresponding to the contours.

V. Conclusion

This paper presented a backwards reachability analysis for spacecraft rendezvous and docking maneuvers around a tumbling object. The scenario included a chief spacecraft in a circular orbit, rotating on its orbit plane at a constant rate. The relative roto-translational dynamics were derived from the tumbling chief's perspective, first for the general case, and simplified for the specific scenario. Instead of attempting to solve the reachability problem, an alternative method was proposed to study reachability characteristics of this high dimensional system using a family of minimum time optimal control solutions. It was shown that the boundary of a backwards reachable set can be visualized through contours of minimum time solutions, on a user-defined subspace. Results presented the minimum time contour plots for both translational and rotational states, and a variety of cases, representing initial conditions from which the specified maneuver is feasible given control and time constraints. The translational subsystem results were fairly straight forward to visualize, and showed expected behaviors. The rotational subsystem was more complex given the nonlinearity of the dynamics, and dimensionality of the state-space. A technique was proposed for visualizing backwards reachable sets of relative attitude using MRPs. Although this technique led to more intuitive visualization, more test points are necessary to gain further insight. Finally, analyzing the reachability characteristics on the angular velocity subspace provided valuable insight on the linear region of the state-space, where a linear approximation may be appropriate. The contributions of this work included a backwards reachability analysis of the 6-DOF system, based on the proposed

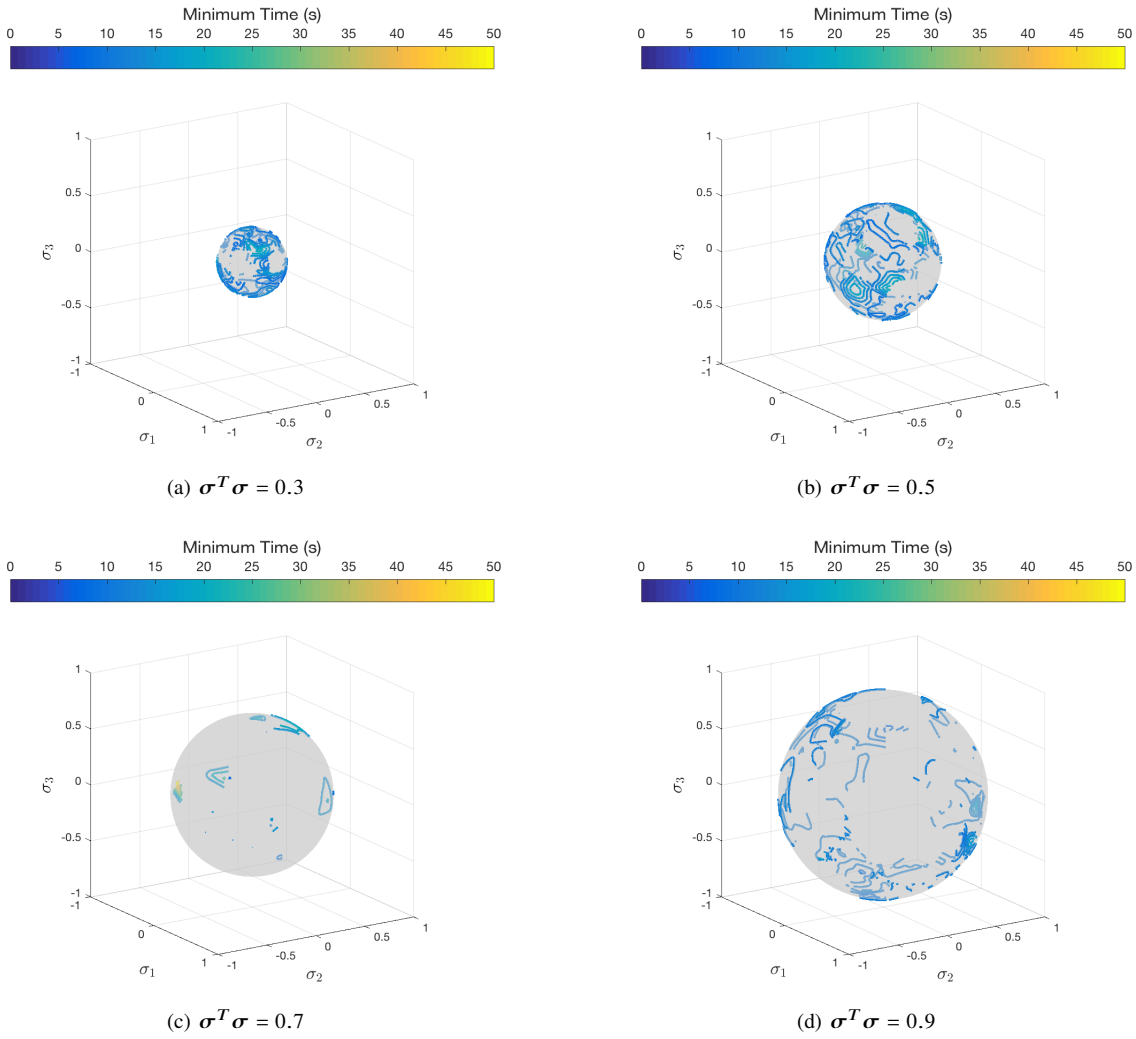

(a) $\boldsymbol{\sigma}^T\boldsymbol{\sigma} = 0.3$ (b) $\boldsymbol{\sigma}^T\boldsymbol{\sigma} = 0.5$

(c) $\boldsymbol{\sigma}^T\boldsymbol{\sigma} = 0.7$ (d) $\boldsymbol{\sigma}^T\boldsymbol{\sigma} = 0.9$

Fig. 8 Rotational backwards T-reachable set slices at zero initial relative angular velocity, at $\Omega = 2\ deg/s$; color bar indicates minimum time values corresponding to the contours.

methodology using minimum time contours in lieu of solving the computationally intensive reachability problem, as well as the visualization technique for attitude sets.

Acknowledgments

All computations for this paper were performed using the Information Technology & Communications Services (ITACS)/High Performance Computing(HPC) cluster, "Hamming", at the Naval Postgraduate School.

References

[1] Ma, Z., Ma, O., and Shashikanth, B. N., "Optimal Control for Spacecraft to Rendezvous with a Tumbling Satellite in a Close Range," *Proceedings of the 2006 IEEE/RSJ International Conference on Intelligent Robots and Systems*, IEEE, Beijing, China, 2006, pp. 4109–4114.

[2] Boyarko, G. A., Yakimenko, O., and Romano, M., "Optimal Rendezvous Trajectories of a Controlled Spacecraft and a Tumbling Object," *Journal of Guidance, Control, and Dynamics*, Vol. 34, No. 4, 2011, pp. 1239–1252. doi:10.2514/1.47645.

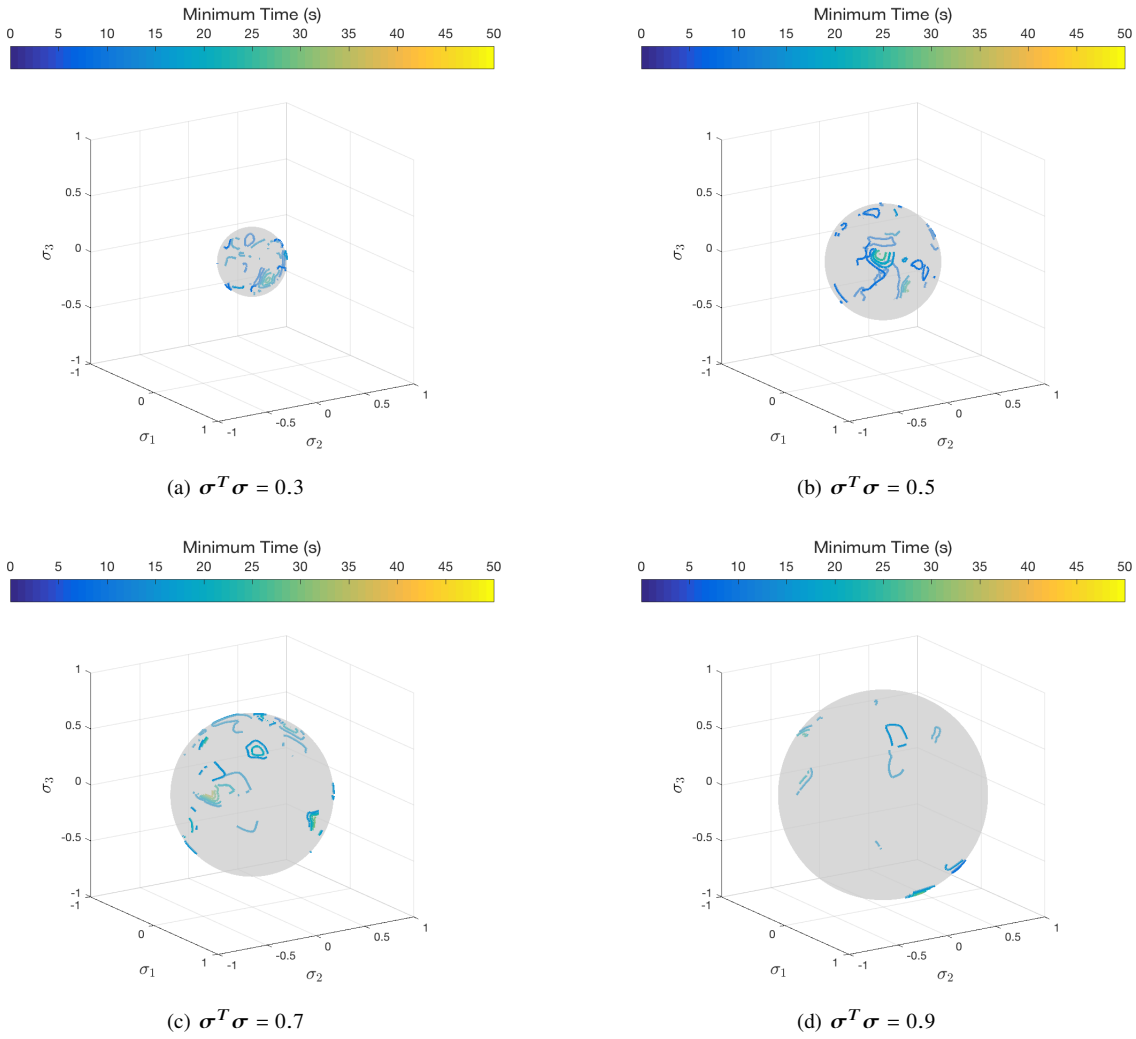

(a) $\boldsymbol{\sigma}^T\boldsymbol{\sigma} = 0.3$ (b) $\boldsymbol{\sigma}^T\boldsymbol{\sigma} = 0.5$

(c) $\boldsymbol{\sigma}^T\boldsymbol{\sigma} = 0.7$ (d) $\boldsymbol{\sigma}^T\boldsymbol{\sigma} = 0.9$

Fig. 9 Rotational backwards T-reachable set slices at zero initial relative angular velocity, at $\Omega = 4\ deg/s$; color bar indicates minimum time values corresponding to the contours.

[3] Boyarko, G. A., "Spacecraft Guidance Strategies for Proximity Maneuvering and Close Approach with a Tumbling Object," Ph.D. thesis, Naval Postgraduate School, Monterey, CA, 2010.

[4] Ventura, J., Ciarcià, M., Romano, M., and Ulrich, W., "Fast and Near-Optimal Guidance for Docking to Uncontrolled Spacecraft," *Journal of Guidance, Control, and Dynamics*, Vol. 40, No. 12, 2017, pp. 3138–3154. doi:10.2514/1.G001843.

[5] Wilde, M., Ciarcià, M., Grompone, A., and Romano, M., "Experimental Characterization of Inverse Dynamics Guidance in Docking with a Rotating Target," *Journal of Guidance, Control, and Dynamics*, Vol. 39, No. 6, 2016, pp. 1173–1187. doi:10.2514/1.G001631.

[6] Xueyan, A., Zhang, R., and Lu, W., "Terminal Sliding Mode Control of Attitude Synchronization for Autonomous Docking to a Tumbling Satellite," *Proceedings of the 2013 International Conference on Mechatronic Sciences, Electric Engineering and Computer (MEC)*, IEEE, Shenyang, China, 2013, pp. 2760–2763.

[7] Sun, L., and Huo, W., "Nonlinear Robust Adaptive Control for Spacecraft Proximity Operations," *Proceedings of the 19th World Congress of the International Federation of Automatic Control (IFAC)*, IFAC, Cape Town, South Africa, 2014, pp. 2219–2224.

[8] Maler, O., "Computing Reachable Sets: An Introduction," Tech. rep., CNRS-VERIMAG, 2008.

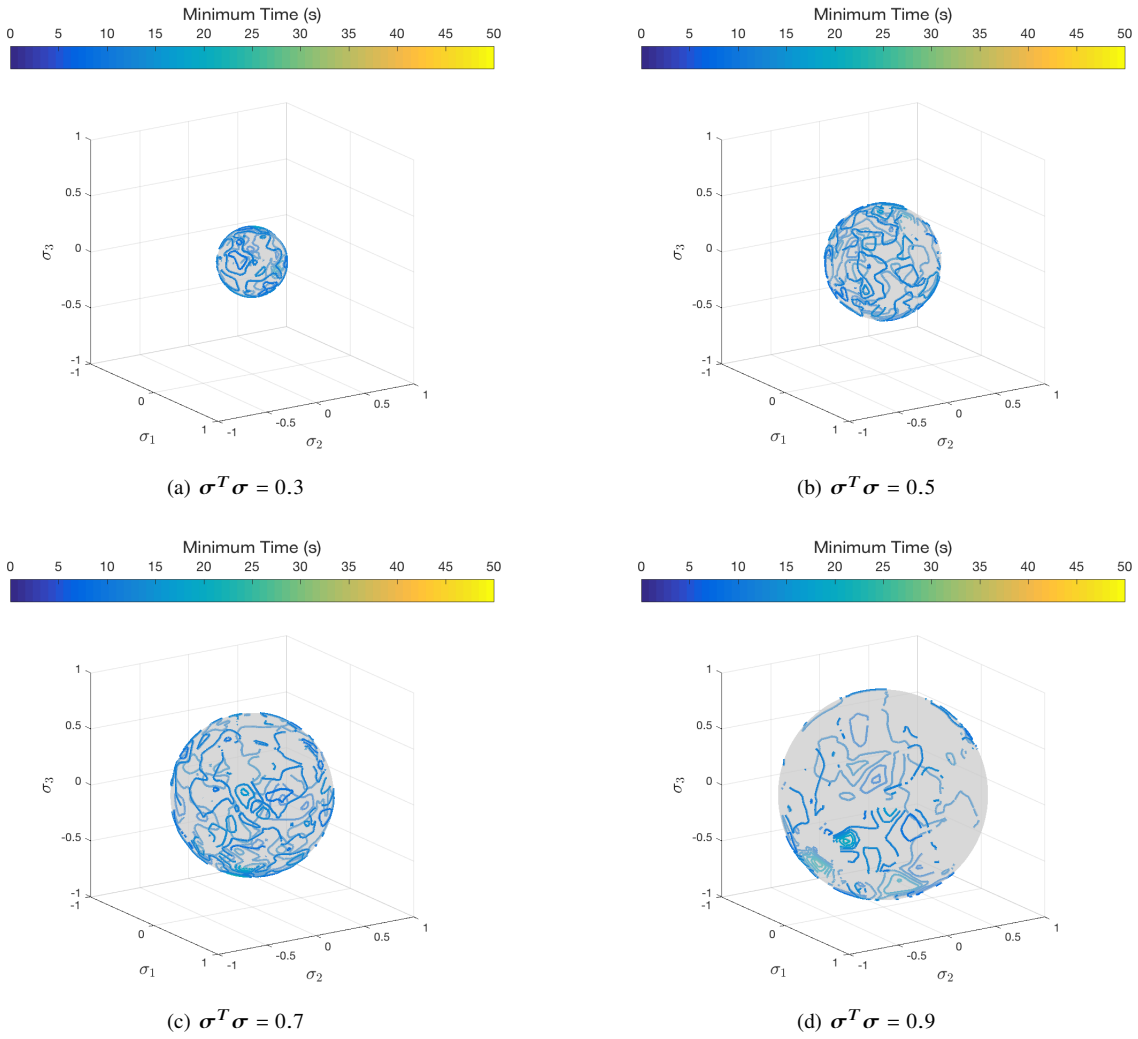

(a) $\boldsymbol{\sigma}^T\boldsymbol{\sigma} = 0.3$

(b) $\boldsymbol{\sigma}^T\boldsymbol{\sigma} = 0.5$

(c) $\boldsymbol{\sigma}^T\boldsymbol{\sigma} = 0.7$

(d) $\boldsymbol{\sigma}^T\boldsymbol{\sigma} = 0.9$

Fig. 10 Rotational backwards T-reachable set slices at zero initial relative angular velocity, at $\Omega = 6\ deg/s$; color bar indicates minimum time values corresponding to the contours.

[9] Bullo, F., and Lewis, A. D., *Geometric Control of Mechanical Systems: Modeling, Analysis, and Design for Simple Mechanical Control Systems*, No. 49 in Texts in Applied Mathematics, Springer, 2005.

[10] Snow, D. R., "Determining Reachable Regions and Optimal Controls," *Advances in Control Systems: Theory and Applications*, Vol. 5, edited by C. T. Leondes, Academic Press Inc., New York, NY, 1967, pp. 133–196.

[11] Dueri, D., Acikmese, B., Baldwin, M., and Erwin, R. S., "Finite-Horizon Controllability and Reachability for Deterministic and Stochastic Linear Control Systems with Convex Constraints," *Proceedings of the 2014 American Control Conference*, AACC, Portland, OR, 2014, pp. 5016–5023.

[12] Lygeros, J., "On Reachability and Minimum Cost Optimal Control," *Automatica*, Vol. 40, No. 6, 2004, pp. 917–927. doi:10.1016/j.automatica.2004.01.012.

[13] Mitchell, I. M., Bayen, A. M., and Tomlin, C. J., "A Time-Dependent Hamilton-Jacobi Formulation of Reachable Sets for Continuous Dynamic Games," *IEEE Transactions on Automatic Control*, Vol. 50, No. 7, 2005.

[14] Mitchell, I. M., and Tomlin, C. J., "Level Set Methods for Computation in Hybrid Systems," *Lecture Notes in Computer Science (LNCS)*, International Workshop on Hybrid Systems: Computation and Control (HSCC '00), Vol. 1790, Springer-Verlag, 2000, pp. 310–323.

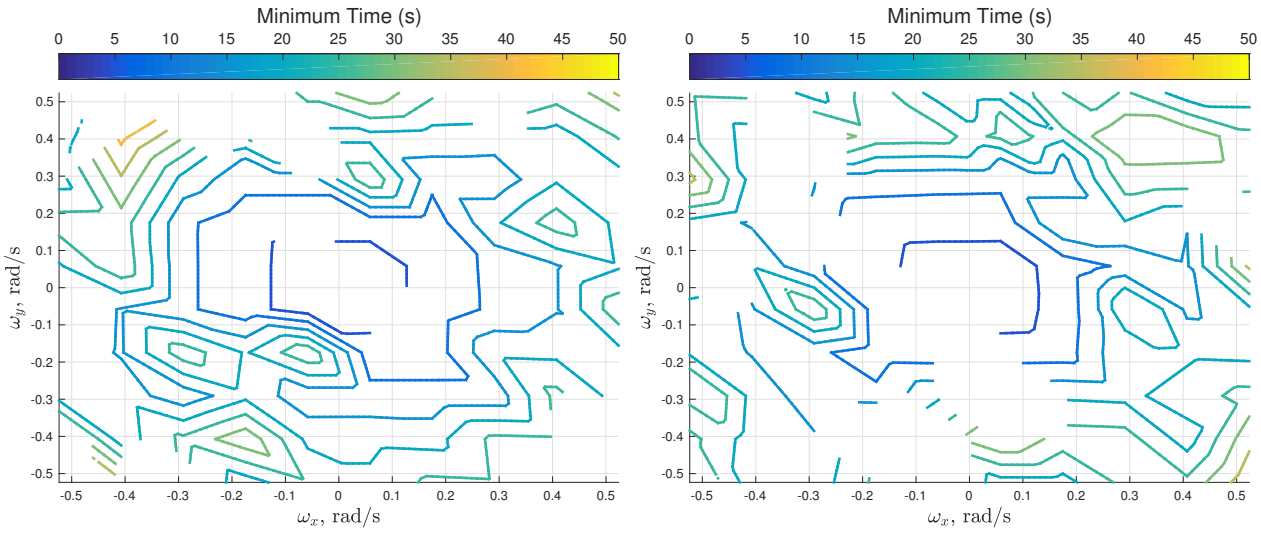

(a) $\Omega = 0\ deg/s$ (b) $\Omega = 2\ deg/s$

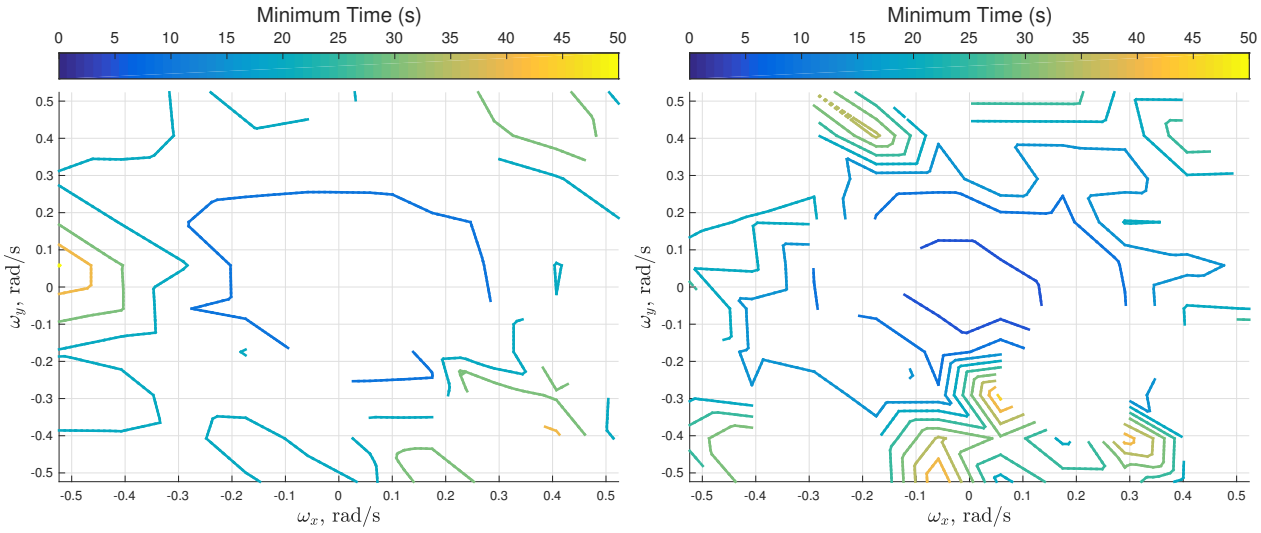

(c) $\Omega = 4\ deg/s$ (d) $\Omega = 6\ deg/s$

Fig. 11 Rotational backwards T-reachable set slices at initially aligned relative attitude and $\omega_z = 0\ deg/s$; color bar indicates minimum time values corresponding to the contours.

[15] Hwang, I., Stipanović, D. M., and Tomlin, C. J., "Polytopic Approximations of Reachable Sets Applied to Linear Dynamic Games and a Class of Nonlinear Systems," *Advances in Control, Communication Networks, and Transportation Systems: In Honor of Pravin Varaiya*, Birkhauser Boston, 2005, pp. 3–19.

[16] Makhlouf, I. B., Hansch, P., and Kowalewski, S., "Comparison of Reachability Methods for Uncertain Linear Time-Invariant Systems," *Proceedings of the 2013 European Control Conference*, EUCA, Zürich, Switzerland, 2013, pp. 1101–1106.

[17] Kurzhanskiy, A., and Varaiya, P., "Ellipsoidal Techniques for Reachbility Analysis of Discrete-Time Linear Systems," *IEEE Transactions on Automatic Control*, Vol. 52, 2007.

[18] Holzinger, M., and Scheeres, D., "Applied Reachability for Space Situational Awareness and Safety in Spacecraft Proximity Operations," *AIAA Guidance, Navigation, and Control Conference*, AIAA, Chicago, IL, 2009.

[19] HomChaudhuri, B., Oishi, M., Shubert, M., Baldwin, M., and Erwin, R. S., "Computing Reach-Avoid Sets for Space Vehicle Docking Under Continuous Thrust," *Proceedings of the 55th Conference on Decision and Control*, IEEE, Las Vegas, NV, 2016, pp. 3312–3318.

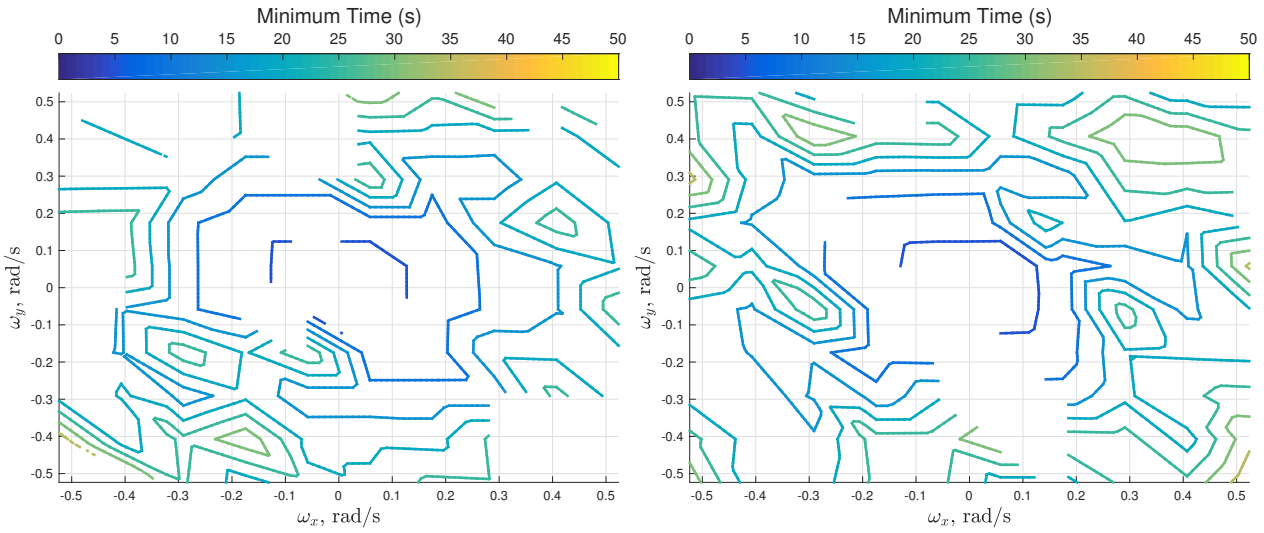

(a) $\Omega = 0\ deg/s$

(b) $\Omega = 2\ deg/s$

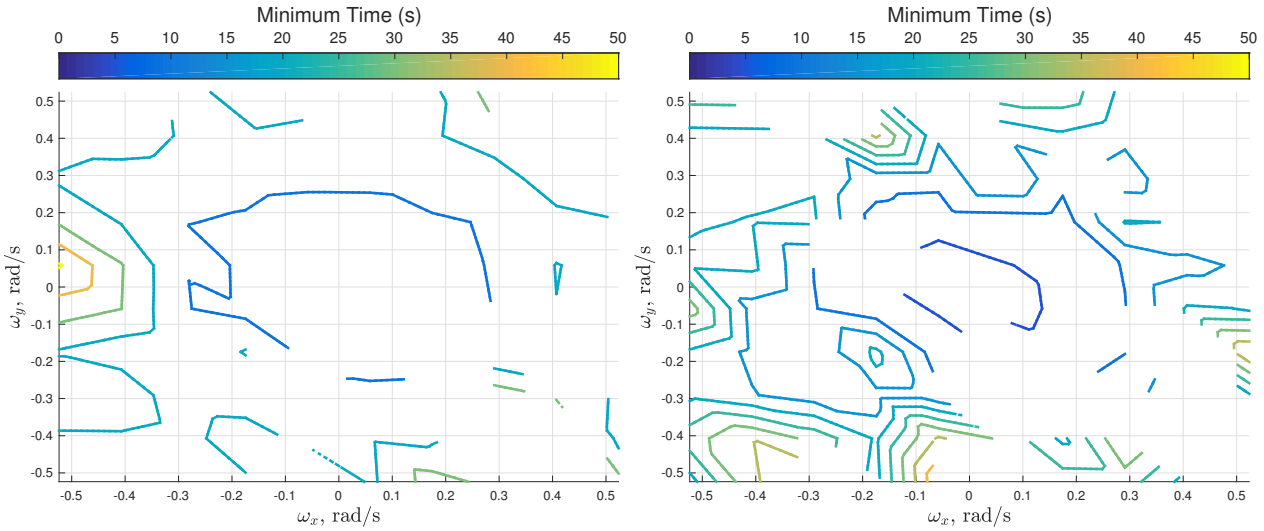

(c) $\Omega = 4\ deg/s$

(d) $\Omega = 6\ deg/s$

Fig. 12 Rotational backwards T-reachable set slices at initially aligned relative attitude and $\omega_z = -15\ deg/s$; color bar indicates minimum time values corresponding to the contours.

[20] Zagaris, C., and Romano, M., "Analysis of Spacecraft Planar Docking with Rotating Body in Close Proximity," *27th AAS/AIAA Spaceflight Mechanics Meeting*, AAS, San Antonio, TX, 2017. URL `http://hdl.handle.net/10945/51980`.

[21] Alfriend, K. T., Vadali, S. R., Gurfil, P., How, J. P., and Breger, L. S., *Spacecraft Formation Flying: Dynamics, Control, and Navigation*, Elsevier Astrodynamics Series, Butterworth-Heinmann, 2010.

[22] Wie, B., *Space Vehicles Dynamics and Control*, 2nd ed., AIAA Education Series, American Institute of Aeronautics and Astronautics, Inc., 2008.

[23] Guarnaccia, L., Bevilacqua, R., and Pastorelli, S., "Suboptimal LQR-based spacecraft full motion control: Theory and Experimantation," *Acta Astronautica*, Vol. 122, 2016, pp. 114–136. doi:10.1016/j.actaastro.2016.01.016.

[24] Segal, S., and Gurfil, P., "Effect of Kinematic Rotation-Translation Coupling on Relative Spacecraft Translational Dynamics," *Journal of Guidance, Control, and Dynamics*, Vol. 32, No. 3, 2009, pp. 1045–1050. doi:10.2514/1.39320.

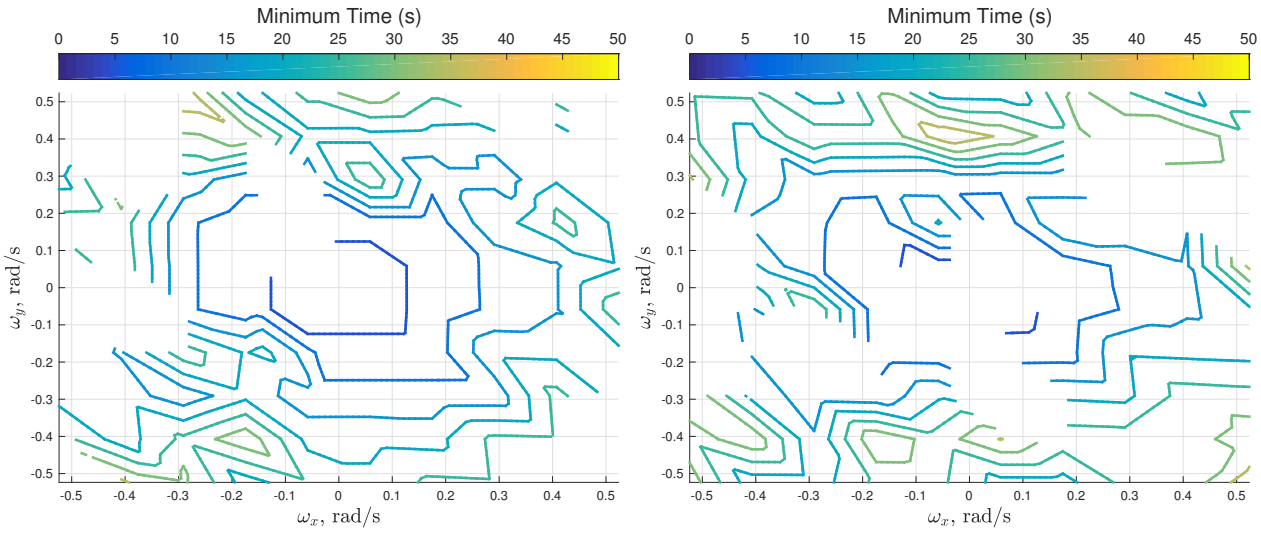

(a) $\Omega = 0\ deg/s$ (b) $\Omega = 2\ deg/s$

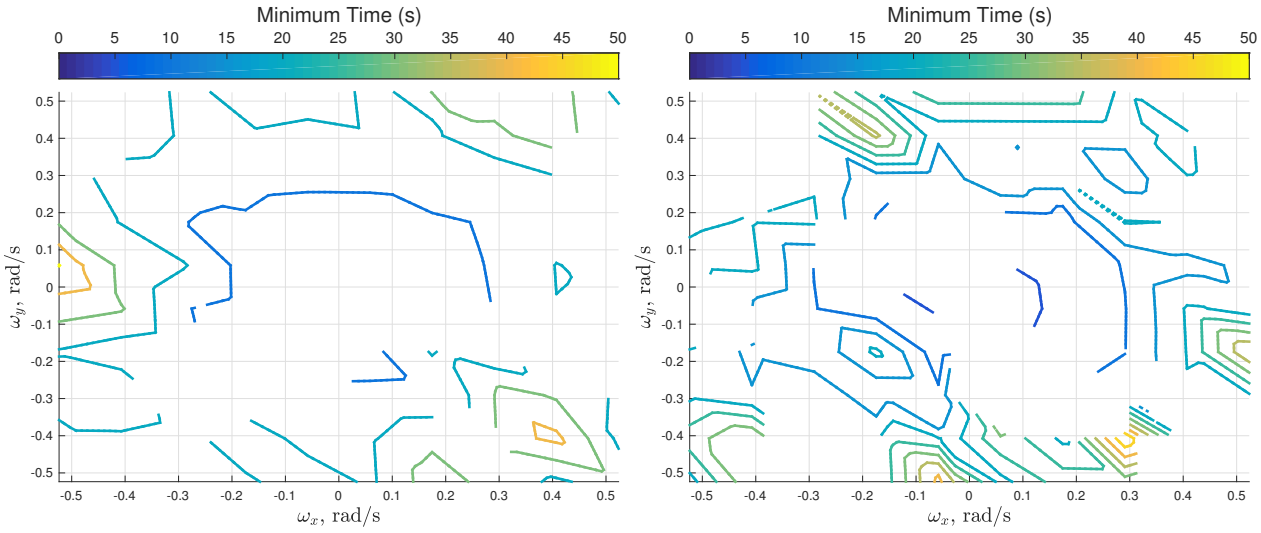

(c) $\Omega = 4\ deg/s$ (d) $\Omega = 6\ deg/s$

Fig. 13 Rotational backwards T-reachable set slices at initially aligned relative attitude and $\omega_z = 15\ deg/s$; color bar indicates minimum time values corresponding to the contours.

[25] Filipe, N., "Nonlinear Pose Control and Estimation for Space Proximity Operations: An Approach Based on Dual Quaternions," Ph.D. thesis, Georgia Institute of Technology, December 2014.

[26] Schaub, H., and Junkins, J. L., *Analytical Mechanics of Space Systems*, American Institute of Aeronautics and Astronautics, Inc., 2003.

[27] Herceg, M., Kvasnica, M., Jones, C., and Morari, M., "Multi-Parametric Toolbox 3.0," *Proceedings of the European Control Conference*, Zürich, Switzerland, 2013, pp. 502–510. `http://control.ee.ethz.ch/~mpt`.

[28] Athans, M., and Falb, P. L., *Optimal Control: An Introduction to the Theory and Its Applications*, McGraw-Hill Book Company, 1966.

[29] Patterson, M. A., and Rao, A. V., *GPOPS-II: A General Purpose MATLAB Software for Multiple-Phase Optimal Control Problems, Version 2.1*, July 2016. URL `http://www.gpops2.com/`.

[30] Shoemake, K., "Uniform Random Rotations," *Graphics Gems III*, edited by D. Kirk, Academic Press, Inc., 1995, pp. 124–132.